Journal of Fluids and Structures (2001) **15,** 641–650
doi:10.1006/jfls.2000.0366, available online at http://www.idealibrary.com on IDEAL®

VORTEX DISLOCATIONS AND FORCE DISTRIBUTION OF LONG FLEXIBLE CYLINDERS SUBJECTED TO SHEARED FLOWS

D. Lucor, L. Imas and G. E. Karniadakis

Center for Fluid Mechanics, Division of Applied Mathematics
Brown University, Providence, RI 02912, U.S.A.

(Received 29 August 2000, and in final form 14 November 2000)

We present DNS results of vortex-induced vibrations (VIV) of flexible cylinders with aspect ratio greater than 500, subjected to linear and exponential sheared flows. The maximum Reynolds number is $\mathrm{Re}_m = 1000$ resulting in a turbulent near-wake. The first case corresponds to lock-in of the third mode ($n = 3$), while the second case is a multi-mode response with excited modes as high as $n = 12$ and 14. We observed vortex dislocations similar to the structures visualized in experiments for stationary cylinders, and obtained corresponding force distributions. Strong vortex dislocations can result in substantial modulation of the forces on the body, and such effects have to be taken into account when constructing low-dimensional predictive models.

1. INTRODUCTION

Previous experimental studies of vibrating cylinders subjected to sheared flows have shown the existence of cellular shedding patterns (Stansby 1976; Woo *et al.* 1981; Peltzer & Rooney 1985). The size and stability of such cells have some subtle differences with similar structures encountered in stationary cylinders, as synchronization (lock-in) and multi-mode response compete directly with frequency mismatching along the span. The latter is the primary reason for the cell formation in either sheared flow or uniform flow past tapered cylinders (Maull & Young 1973; Noack *et al.* 1991; Williamson 1992). The results from the experimental work suggest that the size of the cells is proportional to the amplitude of vibration and inversely proportional to the shear parameter β. This parameter is defined as $\beta = (d/U)(\partial u/\partial z)$, where z denotes the spanwise (cylinder axis) direction, d is the cylinder diameter, and U the span-averaged free-stream velocity. It is possible, therefore, to find cells of constant shedding frequency of 40 diameters or more unlike the stationary cylinder where such cells are not longer than approximately 10 diameters (Peltzer & Rooney 1985).

The experimental work has primarily focused on frequency and point-measurements. However, measurements of forces on the cylinders are needed to establish the effect of vortex dislocations. Such data are currently missing with the exception of recent work by Triantafyllou and collaborators who investigated the effect of vortex splits (Hover *et al.* 1998). In numerical work, the first three-dimensional simulations of VIV of flexible cylinders subjected to sheared flow has been reported in Newman & Karniadakis (1997). Follow-up work including a detailed force distribution for *uniform inflow* was reported in Evangelinos *et al.* (2000). In that work, the difference between a traveling and a standing wave response was examined, and a new empirical model was proposed for predicting the average drag force.

0889–9746/01/040641 + 10 $35.00/0

TABLE 1

FLOW	Linear shear inflow	Exponential shear inflow
Reynolds number (max ~ min)	Re = 1000 ~ 607	Re = 1000 ~ 300
Re = Ud/ν	Turbulent regime	Turbulent/transition regime
Inflow profile	Linear	Gaussian
STRUCTURE	Beam	Beam/cable
Boundary conditions	Pinned and hinged ends	
Constraints	No streamwise motion (x-direction) Free transverse motion (y-direction)	
Aspect ratio, L/d	$L/d = 567$	$L/d = 914$
Mass ratio, m	$m = 2$	$m = 2$
Cable phase velocity, c	$c = 0{\cdot}0$	$c = 25{\cdot}8$
Beam phase velocity, γ	$\gamma = 4487{\cdot}92$	$\gamma = 345{\cdot}248$
Damping, R	$R = 0{\cdot}0$	$R = 0{\cdot}1$

In the current work, we investigate numerically VIV of flexible cylinders subjected to shear flows. We only consider crossflow motion which is described by

$$\frac{\partial^2 Y}{\partial t^2} = c^2 \frac{\partial^2 Y}{\partial z^2} - \gamma^2 \frac{\partial^4 Y}{\partial z^4} - \frac{R}{m}\frac{\partial Y}{\partial t} + \frac{1}{m} F(z,t), \tag{1}$$

where we denote by $Y(z, t)$ the crossflow displacement and by $F(z, t)$ the total lift force, i.e., including both pressure and viscous contributions. Also, m is the mass ratio, R is the damping coefficient, and $c = \sqrt{T/m}$; $\gamma = \sqrt{EI/m}$, where T is the tension and EI the bending stiffness. The lift force is obtained by DNS using the spectral/*hp* element method (Karniadakis & Sherwin 1999), implemented in the parallel code $\mathcal{N}\varepsilon\kappa\mathcal{T}\alpha r$.

In Table 1, we list the values of the parameters in equation (1) for the two main cases we consider in this paper. The first case corresponds to inflow with *linear shear* while the second case corresponds to *exponential shear* described by a Gaussian distribution. The maximum Reynolds number is $\mathrm{Re}_m = 1000$ in both cases and thus a turbulent near-wake is developed. These two cases represent realistic situations corresponding to experimental and field conditions [see references in Furnes (1998) and Allen (1995)]. In equation (1), we refer to the type of structure as a *beam* if $\gamma \neq 0$ and as a *cable* if $c \neq 0$. For the linear shear we examine a beam, and for the exponential shear a mixed beam–cable structure. We also note that unlike most of the previous studies where the aspect ratio of the cylinder was of the order of 100 or less (typically 20–50), here we consider a very large value of aspect ratio (≥ 500, see Table 1).

The numerical simulation and mesh is similar to the one used in Evangelinos & Karniadakis (1999) with 64 points placed along the span, which is sufficient to capture the larger structures only. In order to process spectral information, 64 history points were placed in the near-wake of the cylinder. They are located equidistantly along the span, at the centerline and at $x/d = 3$ in the streamwise direction. Values of velocity and pressure fields are sampled at these history points. Handling such large computational domains requires a great amount of computational resources, especially long-time integration to achieve stationarity of the flow. The only other DNS we are aware of is the work of Vanka and collaborators (Mukhopadhyay *et al.* 1999), who study the laminar wake of a stationary cylinder at an aspect ratio of 24 using a finite volume method.

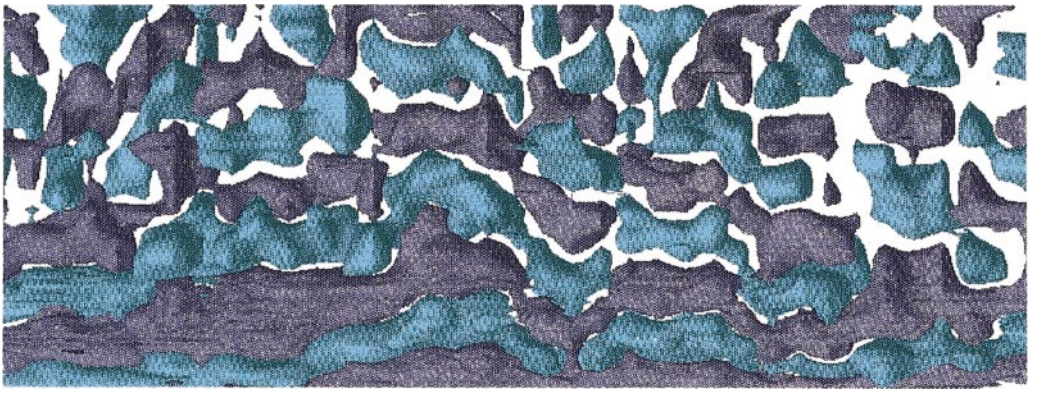

Figure 1. Linear shear case. Iso-contours of crossflow velocity at $\mathrm{Re}_m = 1000$. Only the part corresponding to the large inflow is shown. Dark color: $v = -0{\cdot}2$; light color: $v = 0{\cdot}2$. View normal to the (x, z) horizontal plane, where $80 \leq z/d \leq 400$ and $0 \leq x/d \leq 12{\cdot}5$; flow is upward.

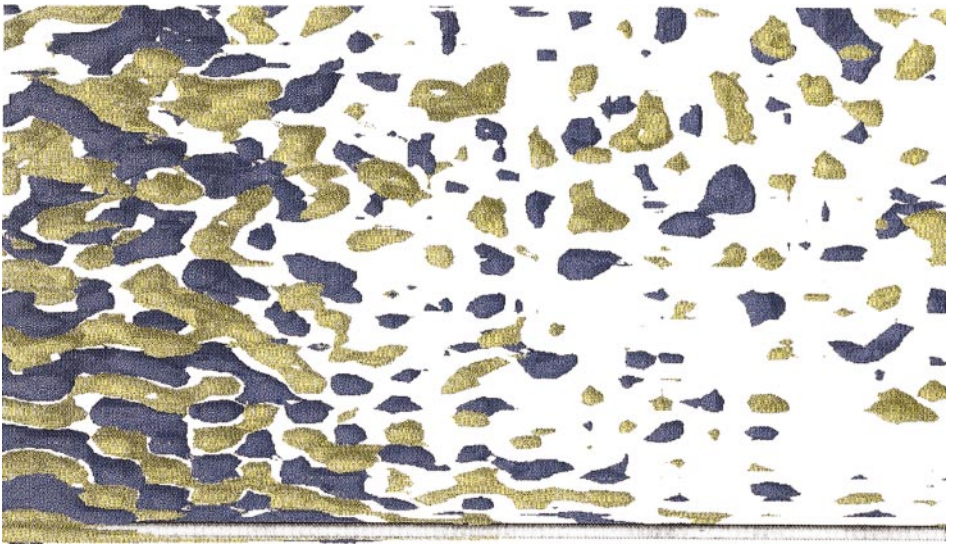

Figure 2. Exponential shear case. Iso-contours of crossflow velocity at $\mathrm{Re}_m = 1000$. Dark color: $v = -0{\cdot}2$; light color: $v = 0{\cdot}2$. View normal to the (x, z) horizontal plane, where $0 \leq z/d \leq 400$ and $0 \leq x/d \leq 35$; flow is upward.

1.1. Visualization of Vortex Dislocations

The most prominent feature observed in shear flow over a bluff body is the shedding of vortices in cells of constant frequency. Because of the mismatch in frequency, vortex dislocations are generated between these cells. The presence of these vortex dislocations in wakes contributes to the transition to turbulence. Vortex dislocations are encountered in transitional and turbulent wakes as well as in laminar wakes, but in a more ordered fashion.

Visualization of vortex dislocations is more clear at low Reynolds number. To this end, we first simulated shear flow past a flexible beam subject to forced and free vibrations for a pinned cylinder of aspect ratio $L/d = 567$ with a mean Reynolds number $\overline{\mathrm{Re}} = 80{\cdot}35$ and a shear parameter $\beta \approx 8{\cdot}8 \times 10^{-4}$; these results and corresponding visualizations were first reported in Lucor *et al.* (2000). The frequency reduces as the *cosine* of the shedding angle (this angle gets steeper as the inflow velocity decreases); similar results were reported for a stationary cylinder in Mukhopadhyay *et al.* (1999). A localized lock-in of the left part of the beam, which corresponds to the side experiencing the large inflow, is obtained. This is similar to the lock-in cell observed in the experiments of Peltzer & Rooney (1985) which extended over 44 cylinder diameters in a cylinder with aspect ratio 107. Here the size of the first cell is larger than that, as both the amplitude of the vibration is larger and the shear parameter is smaller than the experiment [see also Peltzer & Rooney (1985)]. In addition, a significant increase of drag and lift forces was observed in this region of the structure.

The structure, size and dynamics of the dislocations in the case of uniform inflow past a *stationary* cylinder have also been described by Williamson in more recent experimental work (Williamson 1992). He obtained a relationship between the different vortex structures across the boundary between two cells, and explained the interactions between these structures. He also established, in the case of transitional wakes, that the beating frequency of the dislocation between a cell of frequency f_1 and a cell of frequency f_2 is $f_D = f_1 - f_2$. This has successfully been verified in our simulation for a *moving cylinder*, suggesting a universality of vortex dislocations. As regards the fluctuation of cell boundaries, our results confirm the experimental results of Stansby (1976) and Peltzer & Rooney (1985) that vibrations have a stabilizing effect.

Similar visualizations were obtained for a freely moving cylinder. At higher Reynolds number, however, it is more difficult to discern such a clear pattern although a similar picture emerges. For example, for the linear shear flow at $\mathrm{Re}_m = 1000$ we use the crossflow velocity to qualitatively capture instantaneous vortex dislocations in Figure 1. In Figure 2, we plot the crossflow velocity contours in the near-wake for the exponential shear case. We observe a structure much more complex than the linear shear case but with distinct pockets of vortex dislocations, qualitatively similar to the structures we observed in laminar wakes and in linear shear. It is also clear from this plot that the flow does not correlate well along the span of the cylinder, and this invalidates the assumption of full-span correlation employed in the semi-empirical models such as SHEAR7 (Vandiver & Li 1994).

2. VIV FOR LINEAR SHEAR INFLOW

For this simulation the cylinder-to-fluid mass ratio is 2, the structural damping is set to 0·0 in order to obtain a maximum response, and the beam phase speed is set to $\gamma = 4487{\cdot}92$ for lock-in; this corresponds to a natural nondimensional frequency for the beam of 0·1973. For this *linear* shear inflow, the *maximum* Reynolds number (at $z/d = 0{\cdot}0$) and *minimum* Reynolds number (at $z/d = 567$) are 1000 and 607, respectively, with a mean value of 803·5. The shear parameter is $\beta \approx 8{\cdot}8 \times 10^{-4}$, smaller than most of the values used in previous experiments, where $\beta \geq 0{\cdot}005$ [see e.g., Peltzer & Rooney (1985)]. These values are close to

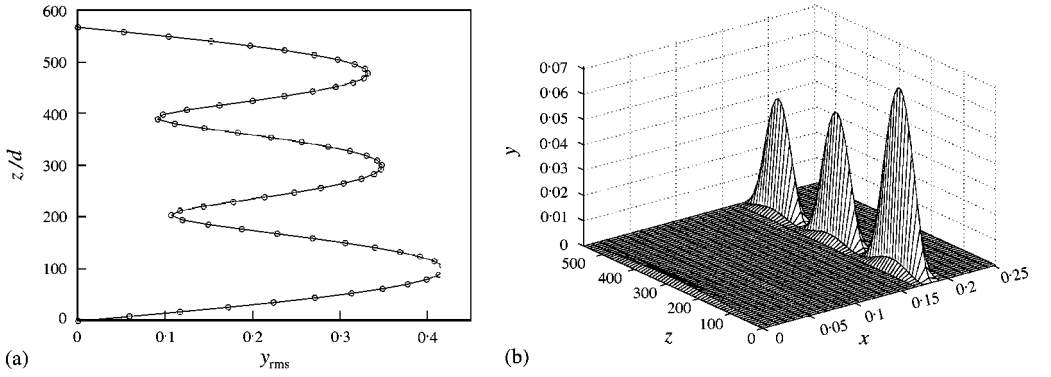

Figure 3. Left: crossflow-displacement (r.m.s. values — horizontal axis) of the beam along the span normalized with the cylinder diameter. Right: corresponding power spectral density (x-axis: frequency nondimensionalized with maximum velocity; y-axis: power spectral density; z-axis: span of the cylinder.

those used in the experiments reported in Furnes (1998) with the exception of Reynolds number, which is lower in the current simulations.

2.1. Displacement and Force Distribution

In Lucor *et al.* (2000), we first reported results for this case; a standing wave response was obtained with the *third mode* excited. The location of the nodes, however, moves somewhat in time, which explains the small but nonzero r.m.s. values of the crossflow displacement. Specifically, a slight shift of these nodes towards the side of the low inflow in the shear inflow case compared to the uniform inflow cases is observed (Evangelinos *et al.* 2000). The standing wave partitions the span of the cylinder in three different cells. The maximum structural response of the beam is reached on the side of the high inflow. Figure 3 displays the standard deviation or r.m.s. values of the vertical displacement of the beam, $(Y(z)/d)_{\mathrm{rms}}$, (normalized by the cylinder diameter), and the spectrum of $(Y(z)/d)_{\mathrm{rms}}$. The maximum r.m.s. value of the crossflow displacement of the beam occurs within the first cell. The r.m.s. structural responses obtained in the second and the third cell are equal even though the beam experiences different inflow velocity. These amplitudes are about 20% lower than the maximum amplitude of the first cell.

The natural frequency of the beam was set to 0·1973, which is the frequency response of a rigid cylinder subject to VIV at a Reynolds number of 1000 (Evangelinos & Karniadakis 1999). If we represent the crossflow motion in the spectral space, we see that only one mode is excited. The structure frequency response is 0·183 (see Figure 3, right). The spectral density is maximum in each cell between the nodes. The wake frequency based on the Reynolds number associated with the mean inflow velocity from the shear inflow for a stationary cylinder is around 0·21 (Fey *et al.* 1998). Therefore, the coupled flow–structure system has a frequency response that deviates towards a smaller value from the imposed frequency, here $f = 0{\cdot}197$, [see also Evangelinos & Karniadakis (1999)].

In Figure 4, we plot the mean values of the drag coefficient, $(C_d(z))_{\mathrm{mean}}$, and r.m.s. values of the lift coefficient along the span of the cylinder. The lift and drag coefficients represented along the span are normalized by the *local* inflow velocity. Due to the shear inflow the local Reynolds number along the span varies from 1000 to 607. The mean value of $C_d(z)$ is about 1·66. The maximum value of $C_d(z)$ takes place at the midspan and its value is 13% larger than the maximum $C_d(z)$ in the case of the uniform inflow [2·1 versus 1·82; see Evangelinos *et al.* (2000)] and 29% larger than the $C_d(z)$ at the same location in the case of the uniform

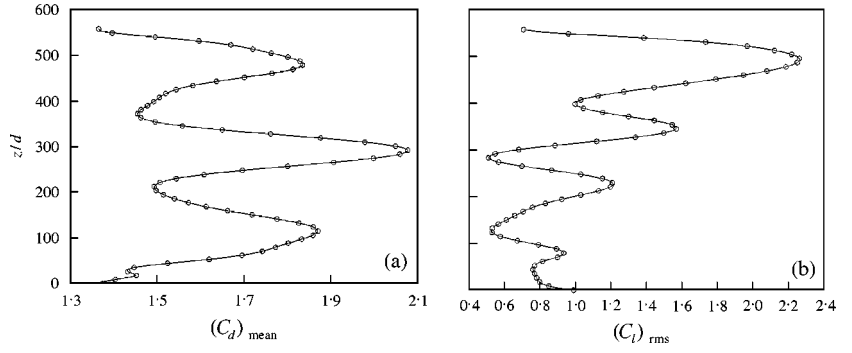

Figure 4. (a) Distribution of $(C_d)_{\text{mean}}$ along the span. (b) Distribution of $(C_l)_{\text{rms}}$ along the span. The local inflow velocity is used in the normalization.

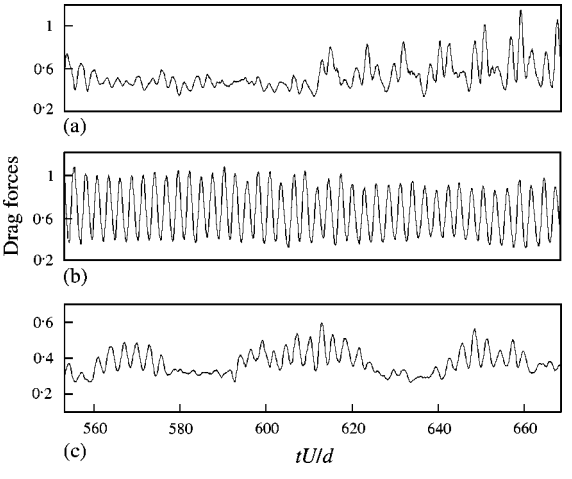

Figure 5. Comparison of time-histories of drag force at different locations along the span: (a) $z/d = 248{\cdot}06$; (b) 283·5; (c) 416·39.

inflow [2·1 versus 1·55; see Evangelinos *et al.* (2000)]. The local minimum values of the $C_d(z)$ are located at the nodes, in agreement with the uniform inflow results (Evangelinos *et al.* 2000).

The plot of $(C_l(z))_{\text{rms}}$ exhibits a large value in the third cell and a small value in the first cell. The response in the central cell is more intriguing and is split into two zones. The overall $(C_l(z))_{\text{rms}}$ along the span has a mean value of 1·12. A maximum value of 2·22 is reached at $z/d = 505$ and a minimum value of 0·35 is achieved at the midspan.

The plot of the lift coefficient can be related to the crossflow motion. The apparent inconsistency between the plots above could be explained by a phase analysis. The spectral density plot (not shown here) of the C_l signal as a function of the frequency shows that only two frequencies are primarily excited. The first one corresponds to the frequency of the beam oscillation ($f = 0{\cdot}183$, see also Figure 3), while the second one is an incomensurate higher frequency ($f = 0{\cdot}296$), which we have not been able to relate to other frequencies. Clearly, the dominant frequency of C_l along the cylinder is $f = 0{\cdot}183$, especially within the third cell where large spectral densities are obtained. We have observed that the C_l signal is in-phase with the beam motion in this cell. This might also explain why the displacement in

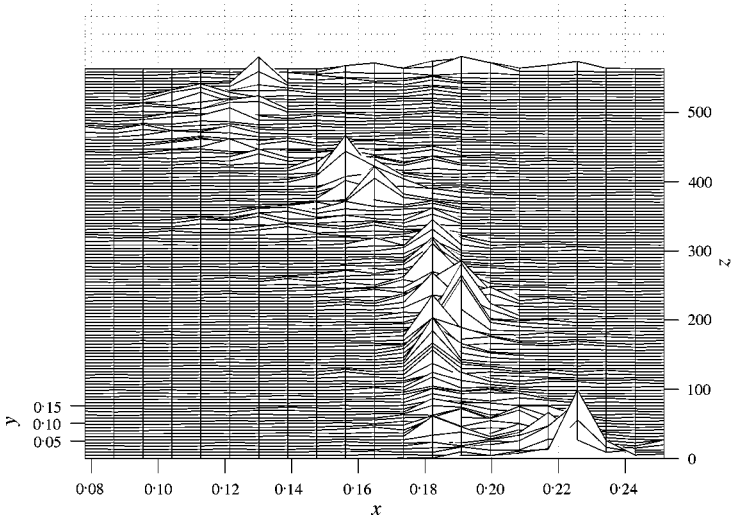

Figure 6. Spanwise (z) power spectral density of the v-component of the velocity field (x-axis denotes frequency nondimensionalized with maximum velocity; y-axis denotes power spectral density, z-axis denotes the span of the cylinder).

the third cell is comparable to the displacement of the second cell even though they experience different inflows.

Finally, in Figure 5 we plot the time histories of the drag force at three different locations along the beam. These positions have been identified after a spectrum analysis of the crossflow v-velocity and streamwise u-velocity (not shown here) in order to locate the positions of the main vortex dislocations. The first plot shows the drag force at $z/d = 248{\cdot}06$, which is the location of the main vortex dislocation of this flow. The second graph is used as a reference and does not reside within a vortex dislocation. Finally, the third graph shows values of drag forces at another vortex dislocation of smaller intensity. There exists a significant *low-frequency modulation* at the first and the third locations compared to the second one. These low frequencies are the same as the leading frequencies of the streamwise u-velocity at these positions.

2.2. Frequency Response

In Figure 6, we plot frequency spectra of the crossflow velocity along the beam. These frequencies can be interpreted as Strouhal numbers based on the *maximum* inflow velocity of the flow ($U_m = 1{\cdot}0$). The most distinguishing feature observed in Figure 6 is the shedding of vortices at constant frequencies. It can be shown that all these peak frequencies are, in fact, linear combinations of the harmonics of $f_1 = 0{\cdot}1996$ with the harmonics of $f_2 = 0{\cdot}2082$, and they can be written in this case as

$$[m - 3(n-1)]\, f_1 + [4(n-1) - m]\, f_2, \tag{2}$$

where $n = 2$ and $m = 1, 2, \ldots, 16$. It is interesting to note that f_1 is very close to the natural frequency for the beam ($f = 0{\cdot}1973$) and f_2 corresponds to the Strouhal number of the flow past a stationary circular cylinder at Reynolds number of 620 (Fey *et al.* 1998). We recall that 607 is the Reynolds number that corresponds to the *minimum* inflow velocity of our shear inflow.

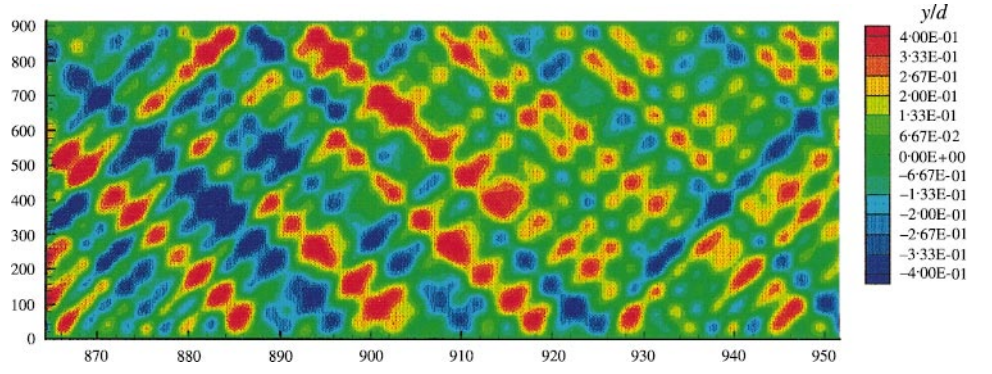

Figure 7. Time-history of the distribution of crossflow displacement along the span. A mixed standing–traveling wave pattern prevails, unlike the linear shear case.

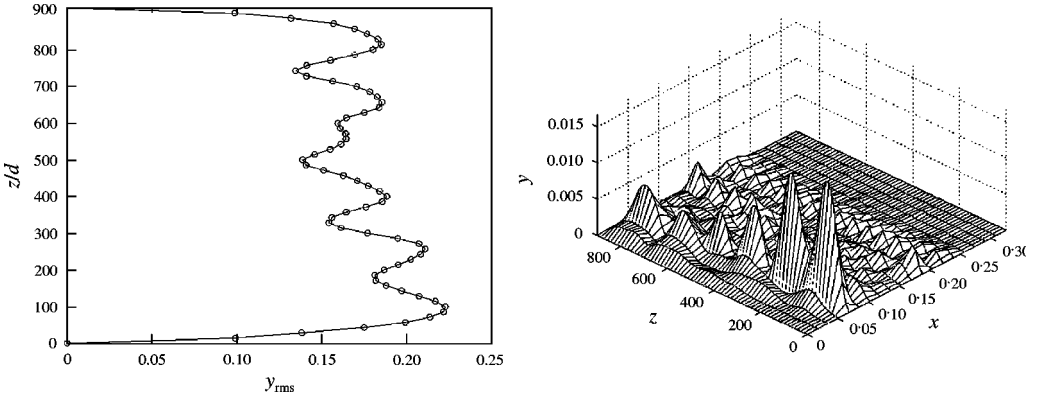

Figure 8. (a) Crossflow displacement (r.m.s. values) along the span (normalized with the cylinder diameter). (b) Corresponding spectrum showing the (nondimensional) frequency response (range: 0–0·3) along the span. The frequency is normalized with the maximum inflow velocity (x-axis: frequency nondimensionalized with maximum velocity; y-axis: power spectral density; z-axis: span of the cylinder).

Barring end-effects that may be induced by possible numerical artifacts, we can distinguish several different frequency cells or frequency ranges. These cells do not match the cells defined by the beam displacement (see Figure 3). The length of these cells is approximately as follows. There is a large first cell from $z/d = 50$ to 250 with a frequency of $f = 0{\cdot}183$, which is the frequency of the crossflow motion of the beam. Then, the second cell lies between $z/d = 250$ and 370 with two frequencies $f = 0{\cdot}183$ and $0{\cdot}165$. A third large cell is between $z/d = 370$ and 425, and the last cell fills the gap between $z/d = 430$ to the end of the beam span. In this case, the spectrum is not very sharp, and it is therefore more difficult to identify the characteristic frequency. Between the cells we notice buffer zones with small spectral density, low energy, e.g. at the midspan, or total energy distributed over a larger number of modes, e.g. at the second-node zone. Clearly, these cells are much larger than the cells encountered in stationary cylinders but this is expected for vibrating cylinders, especially since the shear parameter is very small in our case, and the aspect ratio is very large. The current results are certainly consistent with the experimental results and conclusions reported in Peltzer & Rooney (1985).

3. VIV FOR EXPONENTIAL SHEAR INFLOW

In inflows with large shear the possibility exists for excitation of high modes and of a multi-mode response (Kim *et al.* 1985; Vandiver 1991). This is evident in the case we consider here that corresponds to $\gamma = 345{\cdot}248$ and $c = 25{\cdot}8$ (see Table 1). The corresponding eigenspectrum of a beam–cable structure pinned at both ends is determined by

$$\omega^2 = \gamma^2 k^4 \left[1 + \frac{c^2}{\gamma^2 k^2} \right], \quad k = \frac{n\pi}{(L/d)}, \tag{3}$$

where n is the mode number. Substituting the parameters of Table 1 we obtain a non-dimensional frequency of $0{\cdot}193$ for mode $n = 12$. Given that the Strouhal number at $\mathrm{Re} \sim \mathcal{O}(1000)$ is about $\mathrm{St} \approx 0{\cdot}2$, we verify that indeed the possibility exists for such high modes to be locked-in to the wake.

The specific form of shear profile imposed at the inlet in this case is described by

$$U(z) = (1 - U_f)\, \mathrm{e}^{-a(z/d)^2} + U_f, \quad U_f = 0{\cdot}3, \quad a = 5{\cdot}0 \times 10^{-5} \tag{4}$$

with the high inflow velocity located at $z/d = 0$. The shear parameter in this case is $\beta \approx 0{\cdot}005$.

3.1. Displacement and Force Distribution

In Figure 7, we plot the time-history of the crossflow displacement along the spanwise direction. We see that a mixed response is established, which can be characterized as hybrid between a standing wave and a traveling wave, unlike the linear shear case where a lock-in standing wave pattern was obtained. The r.m.s. values of the crossflow displacement along the span of the cylinder are plotted in Figure 8 (left) along with the corresponding spectrum (right) showing a multi-mode frequency response. Unlike the linear shear case, here the structure oscillates at low frequencies. To investigate further this multi-mode response we obtained the excited modes by analyzing two different instantaneous responses in wavenumber space (plot not shown here). The highest contributing modes are $n = 14$–16 which agree with the results of Triantafyllou *et al.* (1994), a code based on empirical modeling of the flow and eigenfrequency analysis for the structure. The span-averaged value of the crossflow displacement predicted by the current simulation is $0{\cdot}22$ compared to $0{\cdot}243$

obtained by Triantafyllou *et al.* (1994). Also, comparison of the instantaneous response profiles with field measurements (performed on a drilling riser with similar geometric properties and responding to a current with similar shear parameter) between the locations $27 \leq z/d \leq 55$, is very good (Allen 1995). An important difference, already mentioned, between the linear shear response and the exponential shear response is that in the former a standing wave pattern is observed, whereas in the latter a hybrid standing–traveling wave pattern prevails.

3.2. Frequency Response

We have already seen that the beam–cable structure oscillates at a low frequency. This frequency is approximately the same as the low frequency in the wake (plot not shown here) on the low inflow side. In contrast, the lift follows a response similar to the wake on the side of the high-velocity inflow. Therefore, unlike the linear shear case where the frequency response of lift, the wake, and the structure are the same, in the case of exponential shear the lift and the beam–cable response are not the same.

4. SUMMARY AND DISCUSSION

In this paper, we have addressed the effects of linear and exponential shear profiles in VIV of very long flexible cylinders using spectral DNS. The main difference between the two cases is that in linear shear the structural response resembles a standing wave pattern, whereas in the exponential shear case it resembles a mixed standing–traveling wave pattern. For the parameters considered here, the linear shear led to a low-mode (mode 3) response while the exponential shear led to a multi-mode response with modes as high as 12 and 14 participating.

More quantitatively, the difference in the two cases can be summarized in the plots of Figure 9, which include the frequency response of the wake and the structure as well as the natural frequency of the structure. The crossflow velocity at points $(x/d = 3, y/d = 0, z/d)$ is analyzed to obtain the shedding frequency. The most distinguishing feature in these plots is the shedding of vortices at constant frequencies, as it is evident by the values of the Strouhal number which are on parallel lines. This is more pronounced for the linear shear case, for which we also observe that the beam locks on to a wake frequency which dominates on the side of the high inflow. This frequency is lower than the natural frequency of the beam for mode $n = 3$. On the other hand, for the exponential shear we need to consider different modes because of the multi-mode response of the structure. The structure response (non-dimensional) frequency varies from about 0·05 to just above 0·23 with corresponding excited natural modes from $n = 3$ to 12.

We have found that the nodes of the structure are not always located exactly at a boundary between two cells. We also obtained cells of constant shedding frequency, which are much longer than the cells in stationary cylinders reported in experimental work. However, their size is consistent with the experimental results and corresponding conclusions reached in the works of Stansby (1976) and Peltzer & Rooney (1985). It was reported in these works that the size of the cells scales proportionally to the amplitude of crossflow displacement and inversely proportional to the shear parameter. Moreover, we have seen in our simulations that the larger aspect ratio of the flexible cylinder allows for larger cellular patterns. This too is consistent with the experimental results of Peltzer (1982) if we extrapolate from his range of aspect ratio ($L/d \sim 20$–100) to our values ($L/d \sim 567$–914).

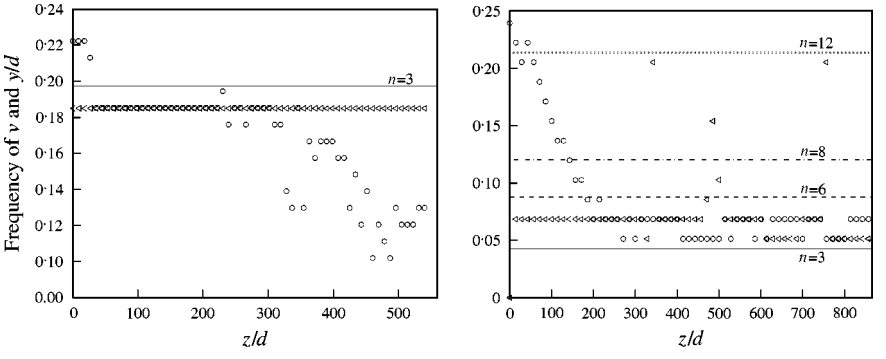

Figure 9. Frequency distribution of wake and structure along the span showing cellular shedding and multi-mode response. (a) linear shear; (b) exponential shear. Circles denote dominant frequency of crossflow velocity and triangles dominant frequency of the structure response. The maximum inflow velocity is used in the normalization of the frequency.

With regards to force distribution on the structure, we have found that vortex dislocations have a significant effect on the *instantaneous* force distributions along the span of the cylinder. The location of vortex dislocations in the wake can best be obtained by searching for energetic low frequencies of the streamwise velocity component (plot not shown here). We have observed that there exists a significant modulation of the forces on the body by these low frequencies at the spanwise locations corresponding to the vortex dislocations. This demonstrates that strong vortex dislocations can have a substantial effect on the forces acting on the body, and such effects have to be taken into account when constructing low-dimensional predictive models.

ACKNOWLEDGEMENTS

This work was supported by the Office of Naval Research, the Department of Energy, and the National Science Foundation. Computations were performed on the NAVO T3E, on the MHPCC SP2, and on the SP Power 3 computer of Brown's Center for Scientific Computing & Visualization. We would like to thank Dr Gunnar Furnes of Norsk Hydro and Dr Owen Oakley of Chevron for useful discussions. We would also like to thank R. M. Kirby and C. Evangelinos for their help with the $\mathcal{N}\varepsilon\kappa\mathcal{T}\alpha r$ code.

REFERENCES

Allen, D. 1995 Vortex induced vibration analysis of the auger TLP production and steel catenary export risers. In *Proceedings Conference on Offshore Technology*, Houston, TX, Paper No. 7821.

Evangelinos, C. & Karniadakis, G. E. 1999 Dynamics and flow structures in the turbulent wake of rigid and flexible cylinders subject to vortex-induced vibrations. *Journal of Fluid Mechanics* **400,** 91–124.

Evangelinos, C., Lucor, D. & Karniadakis, G. E. 2000 DNS-derived force distribution on flexible cylinders subject to VIV. *Journal of Fluids and Structures* **14,** 429–440.

Fey, U., König, M. & Eckelmann, H. 1998 A new Strouhal–Reynolds–number relationship for the circular cylinder in the range $47 < \mathrm{Re} < 2 \times 10^5$. *Physics of Fluids* **10,** 1547–1549.

Furnes, G. 1998 On marine riser responses in time and depth dependent flows. Technical Report, Norsk Hydro, Bergen, Norway.

Hover, F. S., Techet, A. H. & Triantafyllou, M. S. 1998 Forces on oscillating uniform and tapered cylinders in crossflow. *Journal of Fluid Mechanics* **363,** 97–114.

Karniadakis, G. & Sherwin, S. 1999 *Spectral/hp Element Methods in CFD*. New York: Oxford University Press.

Kim, Y.-H., Vandiver, J. & Holler, R. 1985 Vortex-induced vibration and drag coefficients of long cables subjected to sheared flows. In *Proceedings Fourth International Offshore Mechanics and Arctic Engineering Symposium*, New York: ASME.

Lucor, D., Evangelinos, C. & Karniadakis, G. 2000 DNS-derived force distribution on flexible cylinders subject to VIV with shear inflow. In *Proceedings Flow Induced Vibration* (eds S. Ziada & T. Staubli). Rotterdam: A.A. Balkema.

Maull, D. J. & Young, R. A. 1973 Vortex shedding from bluff bodies in shear flow. *Journal of Fluid Mechanics* **60,** 401–409.

Mukhopadhyay, A., Venugopal, P. & Vanka, S. P. 1999 Numerical study of vortex shedding from a circular cylinder in linear shear flow. *Journal of Fluids Engineering* **121,** 460–468.

Newman, D. J. & Karniadakis, G. E. 1997 Simulations of flow past a freely vibrating cable. *Journal of Fluid Mechanics* **344,** 95–136.

Noack, B. R., Ohle, F. & Eckelmann, H. 1991 On cell formation in vortex streets. *Journal of Fluid Mechanics* **227,** 293–308.

Peltzer, R. 1982 Vortex shedding from a vibrating cylinder with attached spherical bodies in linear shear flow. Report 4940, Naval Research Laboratory, Washington, DC, U.S.A.

Peltzer, R. & Rooney, D. 1985 Vortex shedding in a linear shear flow from a vibrating marine cable with attached bluff bodies. *ASME Journal of Fluids Engineering* **107,** 61.

Stansby, P. K. 1976 The locking-on of vortex shedding due to cross stream vibration of circular cylinders in uniform and shear flows. *Journal of Fluid Mechanics* **74,** 641–665.

Triantafyllou, M., Gopalkrishnan, R. & Grosenbaugh, M. 1994 Vortex-induced vibrations in a sheared inflow: A new predictive method. In *Hydroelasticity in Marine Technology* (eds O. Faltinsen *et al.*). Rotterdam: A. A. Balkema.

Vandiver, J. 1991 Dimensionless parameters important to the prediction of vortex-induced vibrations of long, flexible cylinders in ocean currents. MIT Sea Grant Report No. MITSG 91-93, Massachusetts Institute of Technology, Cambridge, MA, U.S.A.

Vandiver, J. & Li, L. 1994 SHEAR7 Program Theoretical Manual. Technical Report, Department of Ocean Engineering, Massachusetts Institute of Technology, Cambridge, MA, U.S.A.

Williamson, C. H. K. 1992 The natural and forced formation of spot–like 'vortex dislocations' in the transition of a wake. *Journal of Fluid Mechanics* **243,** 393–441.

Woo, H., Cermak, J. & Peterka, J. 1981 Experiments on vortex shedding from stationary and oscillating cables in a linear shear flow. Report No. N68305-78-C0055, Naval Civil Engineering Laboratory, Colorado State University, Fort Collins, CO, U.S.A.